Vicinage forces between molecular and atomic fragments dissociated from small hydrogen clusters and their effects on energy distributions

Manuel D. Barriga-Carrasco and Rafael Garcia-Molina

Departamento de Física, Universidad de Murcia, Apartado 4021, E-30080 Murcia, Spain

In this paper we analyze the dynamic evolution of molecular and atomic fragments of small hydrogen clusters interacting with thin solid foils. We compare the vicinage forces, calculated within the dielectric formalism, for H^+, H^0, and H_2^+ fragments. Using a molecular dynamics numerical code we determine the energy distribution of the fragments after interacting with the target. This distribution is compared to experimental results for protons coming from the fragmentation of $v = 2.02$ a.u. H_2^+ ions impinging on an aluminum foil; a fraction of neutral H^0 is needed to be included in the simulation to get a good agreement with the experimental results. The H_2^+ energy spectra for $v = 5.42$ a.u. H_3^+ interacting with amorphous carbon is also determined. The asymmetry in the Coulomb peaks appearing in the energy spectra both experimentally and in our calculation is opposite for H_2^+ than in H^+; kinematic effects and differences in the electronic stopping are enough to reproduce the difference in the alignment of H_2^+ and H^+ fragments.

I. INTRODUCTION

The interaction of molecular beams with solids at $v > v_0$ (Bohr velocity) introduces new insights into the study of projectiles with matter. Molecular projectiles lose their bound electrons and dissociate just after entering the target [1]. The result is a cluster of ions where each of them interacts with the target material and at the same time with the other ions of the cluster [1]. From the analysis of the fragment evolution one can get detailed information on the dynamical properties of the target (induced field, collision rate, etc.). These properties greatly affect the energy distribution of the fragments after they interact with a thin foil, so the study of their energy spectra give the opportunity to compare theoretical models with experimental results.

When a molecular ion moves through a solid without being dissociated it is supposed to be subjected to the same interactions than an atomic projectile, mainly (i) the electronic stopping and straggling and (ii) the collisions with the target nuclei. Once the molecule becomes dissociated additional forces have to be taken into account between the fragments: (iii) Coulomb repulsion and (iv) induced force through the electronic medium of the target, which is known as vicinage force.

In the present work atomic and molecular vicinage forces are analyzed within the dielectric formalism. Fermi [2] was the first to use this formalism to study the interaction of swift charged particles with target electrons. Lindhard [3] obtained an analytical expression for the dielectric function $\epsilon(k, \omega)$ of the stopping medium, which was improved later in a unified theory of the stopping of charged projectiles [4]. Many dielectric function models have been established since then; the ones developed to describe dielectric response of semiconductors [5–7], or the ones developed from the Drude model [8]. Here we use a dielectric function developed by our group that has been optimized for several materials [9–12]. It is based on a linear combination of dielectric functions proposed by Mermin [13] for outer electron excitations,

together with generalized oscillator strengths for inner-shell electron excitations. The parameters entering the Mermin function are derived from a fitting to the experimental energy-loss function (ELF) in the optical limit [9–12].

There are many theoretical and experimental works on vicinage forces that demonstrate that these forces affect the energy loss and charge of fragments dissociated from molecular ions and also tend to align these fragments in the beam direction [14–18] (see Ref. [14] for a complete list of older works). An experimental evidence of the alignment effect is provided by the asymmetric heights of the external peaks that appear in the energy spectra of dissociated fragments [17,19–25]; these peaks are usually known as Coulomb peaks.

Interactions (i)–(iv) have been deeply studied by our research group in the last years [25–29] including a molecular dynamics treatment of the vicinage forces between two neighbor protons. The main aim of this work is to calculate theoretically the vicinage forces between the different types of fragments from small hydrogen clusters and to check this calculation by evaluating, through a simulation code, the asymmetry in the heights of the Coulomb peaks appearing in the fragments energy spectra.

In Sec. II vicinage forces between two general charge densities will be analyzed using the dielectric formalism and specifically calculated between atomic hydrogen species and H_2^+ molecular ions. In Sec. III our molecular dynamics code will be briefly described, and in Sec. IV the computed energy distributions are compared with experimental spectra. Finally, the conclusions are presented in Sec. V. Throughout this work we use atomic units, in other case it will be specified.

II. VICINAGE FORCES

In this section we analyze the vicinage force that a moving particle P_1 with charge density $\rho_{\text{ext1}}(\mathbf{r}, t)$ produces on a second particle P_2 with charge density $\rho_{\text{ext2}}(\mathbf{r}, t)$, when both are embedded in a uniform electron gas characterized by its
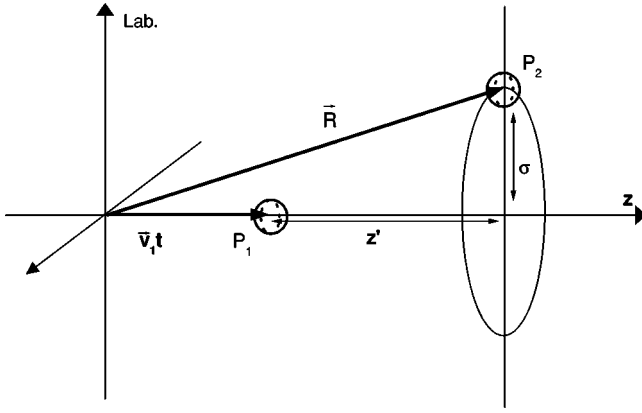
FIG. 1. Parallel z' and perpendicular σ coordinates from the center of the charge density 1 to the center of the charge density 2. Vectors $\mathbf{v}_1 t$ and $\mathbf{R}$ are the positions of the particles 1 and 2, respectively, in the laboratory frame.

dielectric function $\epsilon(k,\omega)$. Following the dielectric formalism, the induced potential $\phi_{\text{ind}}(\mathbf{r},t)$ produced by P_1 is [11]

$$\phi_{\text{ind}}(\mathbf{r},t) = \frac{1}{2\pi^2} \int \frac{d^3k}{k^2} \int d\omega e^{i(\mathbf{k}\cdot\mathbf{r}-\omega t)}$$

$$\times \left[\frac{1}{\epsilon(k,\omega)} - 1 \right] \rho_{\text{ext1}}(\mathbf{k},\omega), \qquad (1)$$

where $\rho_{\text{ext1}}(\mathbf{k},\omega)$ is the Fourier transform of $\rho_{\text{ext1}}(\mathbf{r},t)$.

If P_2 is supposed to move at a constant velocity $\mathbf{v}$ along the z axis (Fig. 1), we have then

$$\rho_{\text{ext1}}(\mathbf{r},t) = \rho_{\text{ext1}}(\mathbf{r}-\mathbf{v}t), \qquad (2)$$

which, in the Fourier space, becomes

$$\rho_{\text{ext1}}(\mathbf{k},\omega) = \int d\mathbf{r} \int dt\, e^{-i(\mathbf{k}\cdot\mathbf{r}-\omega t)} \rho_{\text{ext1}}(\mathbf{r}-\mathbf{v}t)$$

$$= 2\pi\delta(\omega-\mathbf{k}\cdot\mathbf{v})\rho_{\text{ext1}}(\mathbf{k}). \qquad (3)$$

The potential energy of P_2, centered at $\mathbf{R}$, induced by $\phi_{\text{ind}}(\mathbf{r},t)$ is finally

$$\mathcal{E}_{\text{p}}(\mathbf{r},t) = \frac{2}{(2\pi)^5} \int d^3r \int \frac{d^3k}{k^2} \int d\omega e^{i(\mathbf{k}\cdot\mathbf{r}-\omega t)}$$

$$\times \left[\frac{1}{\epsilon(k,\omega)} - 1 \right] \rho_{\text{ext1}}(\mathbf{k},\omega)$$

$$\times \int d^3k' e^{-i\mathbf{k}'\cdot\mathbf{R}} \rho_{\text{ext2}}(\mathbf{k}') e^{i\mathbf{k}'\cdot\mathbf{r}}. \qquad (4)$$

For charge densities with spherical symmetry and using the property $\epsilon(k,\omega) = \epsilon^*(k,-\omega)$ [30], this expression turns into

$$\mathcal{E}_{\text{p}}(z',\sigma) = \frac{2}{\pi v} \int_0^\infty \frac{dk}{k} \int_0^{kv} d\omega J_0(\sigma\sqrt{k^2-\omega^2/v^2})$$

$$\times \rho_{\text{ext1}}(k)\rho_{\text{ext2}}(k) \left\{ \cos(\omega z'/v)\text{Re}\left[\frac{1}{\epsilon(k,\omega)} - 1 \right] \right.$$

$$\left. - \sin(\omega z'/v)\text{Im}\left[\frac{1}{\epsilon(k,\omega)} - 1 \right] \right\}, \qquad (5)$$

where z' and σ are the coordinates of P_2 parallel and perpendicular to P_1 motion in the reference frame centered on P_1 (Fig. 1), and $J_0(x)$ is the zeroth-order Bessel function. We see from Eq. (5) that the potential energy will only depend on z' and σ for a given target material.

The $\mathbf{F}(z',\sigma)$ vicinage force can be derived from the potential energy through

$$\mathbf{F}(z',\sigma) = -\nabla \mathcal{E}_{\text{p}}(z',\sigma). \qquad (6)$$

From Eqs. (5) and (6) the parallel and perpendicular components of this force are written as

$$F_{z'}(z',\sigma) = \frac{2}{\pi v^2} \int_0^\infty \frac{dk}{k} \int_0^{kv} d\omega\, \omega J_0(\sigma\sqrt{k^2-\omega^2/v^2})$$

$$\times \rho_{\text{ext1}}(k)\rho_{\text{ext2}}(k) \left\{ \sin(\omega z'/v)\text{Re}\left[\frac{1}{\epsilon(k,\omega)} - 1 \right] \right.$$

$$\left. + \cos(\omega z'/v)\text{Im}\left[\frac{1}{\epsilon(k,\omega)} - 1 \right] \right\}, \qquad (7)$$

$$F_\sigma(z',\sigma) = \frac{2}{\pi v} \int_0^\infty \frac{dk}{k} \int_0^{kv} d\omega J_1(\sigma\sqrt{k^2-\omega^2/v^2})\sqrt{k^2-\omega^2/v^2}$$

$$\times \rho_{\text{ext1}}(k)\rho_{\text{ext2}}(k) \left\{ \cos(\omega z'/v)\text{Re}\left[\frac{1}{\epsilon(k,\omega)} - 1 \right] \right.$$

$$\left. - \sin(\omega z'/v)\text{Im}\left[\frac{1}{\epsilon(k,\omega)} - 1 \right] \right\}, \qquad (8)$$

where $J_1(x)$ is the first-order Bessel function.

The vicinage force in Eqs. (7) and (8) only include the induced force, not the Coulomb repulsive force. Equations (7) and (8) give the induced force $\mathbf{F}_{1\rightarrow 2}(z',\sigma)$ that P_1 produces on P_2. However $\mathbf{F}_{1\rightarrow 2}(z',\sigma) \neq -\mathbf{F}_{2\rightarrow 1}(z',\sigma)$ because to calculate $\mathbf{F}_{2\rightarrow 1}$ we have to use the velocity of P_2 and the z' and σ coordinates in the P_2 motion reference frame (in the following P_1 will represent the particle that generates the induced field). Vicinage force also depends on the stopping medium through its dielectric function $\epsilon(k,\omega)$.

Putting $z'=\sigma=0$ and $\rho_{\text{ext1}}=\rho_{\text{ext2}}$, $F_\sigma=0$, and $F_{z'}$ yields the self-retarding particle force F_{s}. The variation of the projectile kinetic energy is $dE=\mathbf{F}_{\text{s}}\cdot\mathbf{v}\,dt$ so the electronic stopping S_{e} defined as the energy loss per unit path length becomes

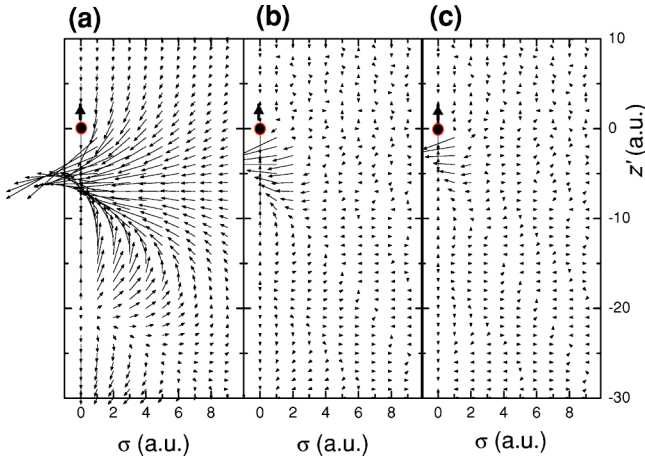$$S_{\text{e}} = \frac{1}{\sigma}\frac{dE}{dt} = -F_{\text{s},z'}(z'=0,\sigma=0). \qquad (9)$$

FIG. 2. Vicinage force generated by a proton, located at $(0,0)$ moving through amorphous carbon in the z' direction with a velocity of $v = 5$ a.u., onto (a) another proton, and (b) an hydrogen atom located at (z', σ). (c) The same for the force generated by a hydrogen atom onto another hydrogen atom. Vector modulus represents the same arbitrary units in the three cases.

Then we get the well-known self-retarding force formula

$$S_e = \frac{2}{\pi v^2} \int_0^\infty \frac{dk}{k} \int_0^{kv} d\omega\, \omega \,\, \mathrm{Im}\left[\frac{-1}{\epsilon(k,\omega)}\right] \rho_{\mathrm{ext}}^2(k). \quad (10)$$

A. Vicinage forces between atomic hydrogen species

In this section vicinage forces between different atomic hydrogen species in solid targets will be calculated. We consider velocities greater than the Bohr velocity, thus H^- can be neglected [31–34] and only H^+ and H^0 are taken into account. The effects of these vicinage forces in the energy spectra at zero angle of the different hydrogen species that exit the solid foils will be simulated and compared to experiments later on.

To calculate these vicinage forces one has to substitute into Eqs. (7) and (8) the Fourier transform of the appropriate charge densities corresponding to the fragments dissociated from the molecular ion. There are three kinds of vicinage forces between H^+ and H^0 fragments: namely, those corresponding to the couples H^+-H^+, H^+-H^0, and H^0-H^0.

For the simplest case, the vicinage force that a H^+ produces on another H^+, we have $\rho_{\mathrm{ext1}}(k) = \rho_{\mathrm{ext2}}(k) = 1$. The result of this force can be seen in Fig. 2(a) when the velocity is $v = 5$ a.u. and the target is amorphous carbon, whose $\epsilon(k,\omega)$ has been calculated in Ref. [11]. This vicinage force presents an oscillatory behavior behind P_1, with a wavelength $\lambda \sim v/\omega_{\mathrm{pl}}$ (where ω_{pl} is the plasmon frequency of the material). This oscillation is damped because the plasmon lifetime is not infinite, which is taken into account in Mermin dielectric function [13] through a collision term. On the other hand, vicinage force decays transversely almost exponentially. Then it is clear that the neighboring particle P_2 will experience a stopping or an accelerated force according to its coordinates (z', σ) regarding the position and velocity of P_1. The parallel component $F_{z'}$ will cause stopping or accelera-

tion of P_2, while the perpendicular component F_σ will cause a change of direction.

The case of the force that a H^+ creates on a H^0 and vice versa can be found in the same way as the H^+-H^+ vicinage force but taking into account that one of the charge densities is a H^+ and the other one is a H^0. In this work it will be supposed that the hydrogen atom is in its ground state, because the population of excited states is very small in our velocity range [35], and this ground state is unperturbed. Thus the charge density of the hydrogen atom in the Fourier space is given by

$$\rho_{\mathrm{ext}}(k) = 1 - \rho_{\mathrm{el}}(k), \quad (11)$$

where the Fourier transform of the electronic density in the ground state is

$$\rho_{\mathrm{el}}(k) = [1 + (k/2)^2]^{-2}. \quad (12)$$

Figures 2(b) and 2(c) show H^+-H^0 and H^0-H^0 vicinage forces for a velocity $v = 5$ a.u. in amorphous carbon, respectively. To calculate the H^+-H^0 force, charge densities $\rho_{\mathrm{ext1}}(k)$ and $\rho_{\mathrm{ext2}}(k)$ have been substituted by 1 and by Eq. (11) into Eqs. (7) and (8), respectively. To calculate the H^0-H^0 force both charge densities $\rho_{\mathrm{ext1}}(k)$ and $\rho_{\mathrm{ext2}}(k)$ have been substituted by Eq. (11) into Eqs. (7) and (8). Comparing Figs. 2(a) and 2(b), we see a substantial difference in the modulus of the forces and in the wavelength of the oscillations of the force direction. Figure 2(c) shows that the H^0-H^0 force is insignificant in relation to the H^+-H^+ and H^+-H^0 forces, except for $-15 < z' < 0$ a.u., and in the σ direction beyond $\sigma = 4$ a.u. The H^+-H^0 force has less intensity and range than the H^+-H^+ one, which is due to the electronic density of the hydrogen atom. And in its turn, the H^0-H^0 force has smaller intensity and range than the H^+-H^0 one, due to the electronic density of the two hydrogen atoms.

B. Vicinage forces between a molecular H_2^+ ion and an atomic hydrogen species

This section studies the electronic vicinage forces between a H_2^+ ion and an atomic hydrogen species. To calculate the vicinage forces in these cases, the Fourier transform of the H_2^+ ion charge density, $\rho_{\mathrm{ext}}(\mathbf{k})$, is needed. Supposing that the H_2^+ electronic density is mostly in the ground molecular level $\sigma_g 1s$ and considering Gaussian wave functions to describe this level, we have [36]

$$\rho_{\mathrm{extH_2^+}}(\mathbf{k}) = [Z_1 - N_G^2 e^{-k^2/8\alpha}] e^{-i\mathbf{k}\cdot\mathbf{P}/2}$$

$$+ [Z_1 - N_G^2 e^{-k^2/8\alpha}] e^{i\mathbf{k}\cdot\mathbf{P}/2} - N_G^2 e^{-k^2/8\alpha} 2 e^{-\alpha P^2/2},$$

$$(13)$$

where $Z_1 = 1$ is the charge of each proton of H_2^+ nucleus, $\mathbf{P}$ is the internuclear vector (which modulus is $P = 2.05$ a.u.), $\alpha = 0.43$ a.u. is the electronic orbital parameter, and N_G is the normalization factor for the electronic molecular orbital:

$$N_G = \left\{ \frac{1}{2[1 + \exp(-\alpha P^2/2)]} \right\}^{1/2}. \tag{14}$$

As the Fourier transforms of the ion charge densities in Eqs. (7) and (8) depend only on the modulus of $\mathbf{k}$, we can divide $\rho_{extH_2^+}(\mathbf{k})$ in three spherical charge densities centered at different positions in the real space (as $e^{-i\mathbf{k}\cdot\mathbf{R}}$ represents an $\mathbf{R}$ displacement in the real space), i.e.,

$$\rho_{extH_2^+}(\mathbf{k}) = \rho_{H_2^+I}(k)e^{-i\mathbf{k}\cdot\mathbf{P}/2} + \rho_{H_2^+I}(k)e^{i\mathbf{k}\cdot\mathbf{P}/2} + \rho_{H_2^+II}(k), \tag{15}$$

where $\rho_{H_2^+I}(k) = Z_1 - N_G^2 e^{-k^2/8\alpha}$ and $\rho_{H_2^+II}(k) = -N_G^2 e^{-k^2/8\alpha} 2 e^{-\alpha P^2/2}$. So the vicinage force of a H_2^+ ion on H^+ can be expressed as

$$\mathbf{F}_{H_2^+ - H^+}(\mathbf{r},t) = \mathbf{F}_I(\mathbf{r} - \mathbf{P}/2,t) + \mathbf{F}_I(\mathbf{r} + \mathbf{P}/2,t)$$

$$+ 2e^{-\alpha P^2/2}\mathbf{F}_{II}(\mathbf{r},t), \tag{16}$$

where $\mathbf{F}_I$ is the vicinage force between charge densities $\rho_{ext1}(k) = \rho_{H_2^+I}(k)$ and $\rho_{ext2}(k) = 1$, whereas $\mathbf{F}_{II}$ is the vicinage force between charge densities $\rho_{ext1}(k) = \rho_{H_2^+II}(k)$ and $\rho_{ext2}(k) = 1$.

When a H_2^+ ion moves inside a target material its internuclear vector orientation is random, and although considering the modulus of the internuclear vector constant ($|\mathbf{P}| = P = 2.05$ a.u.), their components, $P_\parallel$ and $P_\perp$, are not. Vicinage force will depend on the H_2^+ internuclear vector orientation so in our computer code we draw it randomly each time we calculate this force.

The vicinage force $\mathbf{F}_{H_2^+ - H^+}$ is depicted in vectorial form in Fig. 3 for the case when the internuclear vector of the H_2^+ ion is parallel to its velocity. This force has a similar magnitude but an extended shape as compared to the vicinage force between two protons reported in Fig. 2(a). Also we can see that $\mathbf{F}_{H_2^+ - H^+}$ has two characteristic minimum values at the proton positions of the H_2^+ molecular ion.

To conclude this section, it is worth to remark that the same procedure can be used to calculate vicinage forces between any complex molecules if their charge densities can be treated as a combination of spherical charge densities.

III. SIMULATION CODE

Our research group has developed a numerical code to follow the trajectories of the fragments dissociated from molecular ions, which has been described elsewhere [25,28,37]. Here it is summed up in a few conspicuous points featuring this work.

Inside the target the molecular ion moves first without dissociating, and secondly dissociated into its fragments. The time traveling nondissociated is drawn from the lifetime of the molecule [38–41]. The electronic stopping and straggling are calculated through the dielectric formalism, as it was done with the vicinage forces in the last section [36,37]. Nuclear collisions are computed adapting a Monte Carlo al-
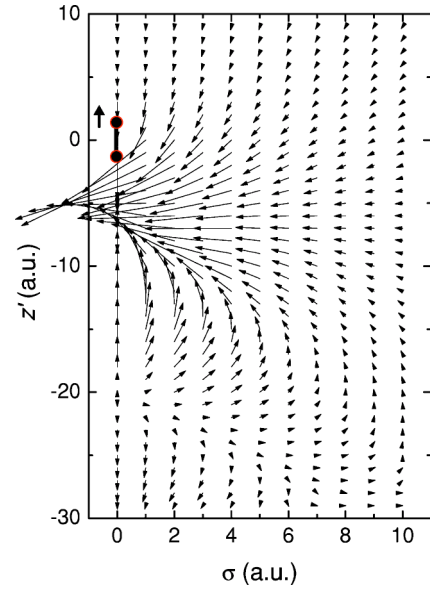

FIG. 3. Force generated by a H_2^+, located at (0,0) moving in amorphous carbon in the z' direction with a velocity $v = 5$ a.u., on a proton located at (z',σ). The H_2^+ internuclear vector is oriented in the z' direction. Vector modulus represents the same arbitrary units as in Fig. 2.

gorithm developed by Möller et al. [42] involving the classical theory of the angular dispersion and elastic energy loss with a Thomas-Fermi Coulomb screened potential and the universal screening distance [43]. After the dissociation of the molecule, the fragments suffer Coulomb repulsions and the vicinage forces explained in Secs. II A and II B. The effect of coherent scattering was shown to represent a small correction to other effects in this velocity range [28] so it is left out of our calculations.

The initial geometry of each molecular ion has been taken into account because the forces between fragments depend strongly on the modulus and on the orientation of the internuclear vectors regarding to the motion direction of the beam. For the case of H_2^+, the initial internuclear distance is drawn from an internuclear distribution theoretically calculated using the Franck-Condon principle [44]. The initial internuclear distances for H_3^+ molecular ions are drawn from experimental internuclear distributions [20,21]. Besides, the initial geometry of the molecule is characterized by a orientation obtained from a random draw of Euler angles.

The simulation code uses a standard molecular dynamics method to follow the evolution of a system of particles, using a numerical integration of Newton equations. It is also considered in a simple way the possibility that the fragments can capture or lose an electron inside the foil to account for the different vicinage forces. In order to implement these processes in the computer code, the charge of each particle has been chosen randomly at each time step of the numerical integration of Newton equations, according to the equilibrium charge fraction corresponding to its velocity [34]. For our velocity range, H^+ and H^0 have different electronic stopping but the same differential scattering cross section for ion-ion collision. On the other hand H_2^+ electronic stopping

is smaller than twice the proton one [36] and the same differential scattering cross section as a D^+ ion. Also vicinage forces depend of the charge state of the two fragments as it has been studied in Secs. II A and II B. Coulomb repulsion are taken into account only between positive fragments inside and also outside the foil. Considering Coulomb repulsion outside thin foils is important because Coulomb explosion inside the target is not complete, especially at highest fragment velocities. The trajectories are calculated until the projectile reaches the detector, and the experimental angular acceptance is taken into account in order to consider the effects of a finite resolution detector.

IV. RESULTS

When a molecular ion is dissociated in two positive fragments, the energy spectrum at zero exit angle of these two fragments is characterized by a lower- and a higher-energy peak. These peaks correspond to the fragments that are retarded or accelerated, respectively, due to Coulomb repulsion, so they are called Coulomb peaks. The asymmetric heights of the Coulomb peaks are due to the asymmetry of the vicinage force, which tend to align the neighbor fragments in the velocity direction. As the vicinage force is more intense behind the fragment that generates the force, the trailing fragment tends to be aligned behind the leading fragment motion direction and so the lower-energy Coulomb peak becomes more intense in the energy spectra [17,19–25,28].

In what follows we will analyze H^+ and H^0 vicinage force effects in the energy distribution of H^+ ions dissociated from H_2^+ ions, and H_2^+, H^+, and H^0 vicinage force effects in the energy distribution of H_2^+ ions dissociated from H_3^+ ions.

A. Vicinage force effects in the energy distribution of H^+ ions

In order to analyze the vicinage forces between atomic hydrogen species, simulated energy distributions of the proton fragments dissociated from H_2^+ molecules are compared with the corresponding experimental spectrum [45]. Specifically, these energy distributions are calculated for incident H_2^+ molecules with $v = 2.026$ a.u. and exiting in the forward direction (i.e., at $0°$ angle with respect to the axis of incidence) after traversing a 360 a.u. thick aluminum foil, whose $\epsilon(k,\omega)$ has been calculated in Refs. [10,11]. These velocities are chosen because the fraction Φ_0 of hydrogen atoms in the dissociated fragments is high enough, $\Phi_0 \simeq 20\%$ [34], to observe the vicinage force effects of this species.

We represent in Fig. 4 the experimental data [45] by symbols while the set of histograms pertain to simulations with different values of the neutral charge fraction Φ_0, as indicated. All distributions are normalized to unit area.

It can be seen from the simulations that if the neutral charge fraction is zero, $\Phi_0 = 0$ (i.e., the two fragments are protons), two peaks are obtained in the energy distributions, which correspond to the protons that are retarded or accelerated due to the Coulomb repulsion. Also a difference in height of these two peaks is observed due to the alignment effect of vicinage forces between the protons. However the
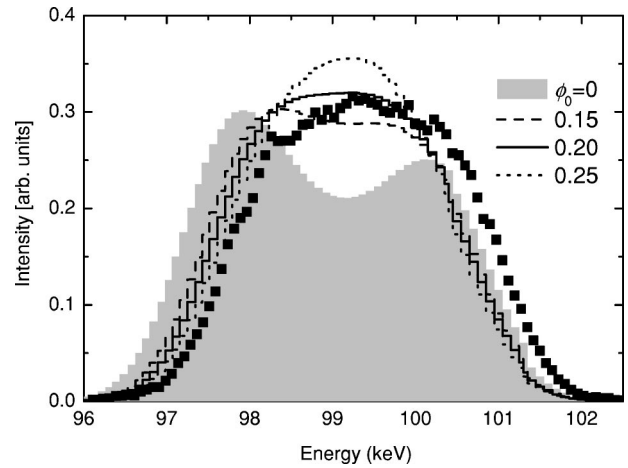

FIG. 4. Energy spectrum at zero exit angle of proton fragments of H_2^+ molecules after traversing a 360 a.u. thick aluminum foil, together with the experimental data [45] (symbols). The incident molecule velocity is 2.026 a.u. The four simulation histograms correspond to different values of the neutral charge fraction Φ_0.

experimental distribution does not show the double-peak structure obtained from the simulation in the $\Phi_0 = 0$ case, which means that Φ_0 has a strong influence on the energy distribution of the H^+ fragments.

When the neutral charge fraction is increased in simulations, the path fraction in which both fragments travel as H^+ diminishes and so the action of the Coulomb repulsion is reduced, leading to a narrower energy distribution as it is observed in Fig. 4. Also there is an increase of those particles that did not experience repulsion at all, increasing the central region of the energy distributions [19,22,46,47]. Finally one can see that the peak height difference diminishes due to the fact that vicinage force effects for neutrals are lower than for protons. From these simulations it seems apparent that a neutral fraction $\Phi_0 \simeq 20\%$ provides the best agreement with the data, in accordance with the neutral fraction found in experiments [34], and part of this agreement is due to the inclusion of the vicinage forces of the hydrogen atoms in our calculations.

B. Vicinage force effects in energy distributions of H_2^+ ions

To study the vicinage force effects in the case of H_2^+ ions, the experimental energy spectrum of H_2^+ ions resulting from the dissociation of the H_3^+ ions is discussed in what follows.

Figure 5 displays the experimental energy spectrum [48] (symbols) of H_2^+ ions that exit a 172 a.u. thick amorphous carbon foil in the forward direction. The H_2^+ ions are created by fragmentation of a H_3^+ ion beam incident with an initial velocity $v = 5.42$ a.u. The energy spectrum shows three peaks: the two external (and greater) peaks are the result of the Coulomb repulsion between dissociated positive pair fragments, $H_2^+ + H^+$, while the smaller central peak is due to the lack of this repulsion between the dissociated pair fragments $H_2^+ + H^0$.
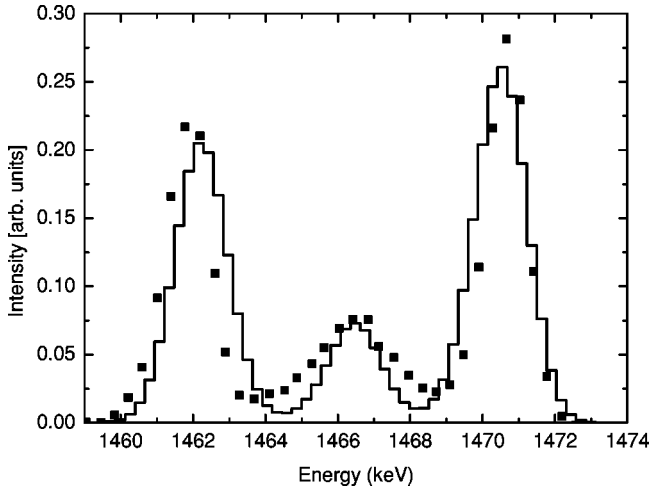
FIG. 5. Energy spectrum at zero exit angle of H_2^+ ions transmitted through a 172 a.u. thick amorphous carbon foil, dissociated from H_3^+ ions incident with 5.42 a.u. velocity. Symbols represent experimental results [48] and the histogram is our calculation.

The most outstanding feature in these Coulomb peaks is that the lower-energy peak is smaller than the higher-energy peak, opposed to what is seen in the energy spectrum of the atomic fragment, Fig. 4. This feature was pointed out by Cue *et al.* [48], as due to an asymmetric destruction process of H_2^+ ions in the solid; these authors explained that as H_2^+ ion destruction is mainly due to the interactions with target valence electrons, the larger target electron density induced behind a leading positive charge supposes an increased probability for trailing H_2^+ ion destruction, which results in a less intense lower-energy peak.

To check the arguments by Cue *et al.*, we have compared in Fig. 5 our simulation results (full line) with their experimental data (symbols), obtaining a good agreement with experiments, in particular concerning the asymmetry of the Coulomb peaks. This result has been obtained without introducing any H_2^+ destruction increasing factor induced by the neighbor positive charge. Thus other effects have to be analyzed.

The asymmetry of the Coulomb peaks could be due to the fact that electronic stopping per amu ($S_{em}=S_e/m$) of the H_2^+ ion is smaller than the one of H^+; $S_{emH_2^+}/S_{emH^+}$ $=0.77$ for this specific velocity [36,37]. So after the H_2^+ $+H^+$ dissociation, the H_2^+ velocity will become larger than the H^+ one and H2+ ions will travel in front of its H^+ partner resulting in a extra accumulation of H_2^+ ions at the higher energies. This effect can be estimated in our simulation code by putting the electronic stopping per amu of H^+ ions equal to the H_2^+ value in the $H_2^++H^+$ dissociation. From the result depicted in Fig. 6(a) (full line), we see that the height asymmetry of the Coulomb peaks has decreased compared to the former simulation, Fig. 6(a) (shadow histograms), but has not disappeared; so the electronic stopping influences the peak asymmetry but it is not the only responsible.

Another cause could be due to the H_2^+-H^+ vicinage force commented in Sec. II B. We calculated the energy distribu-
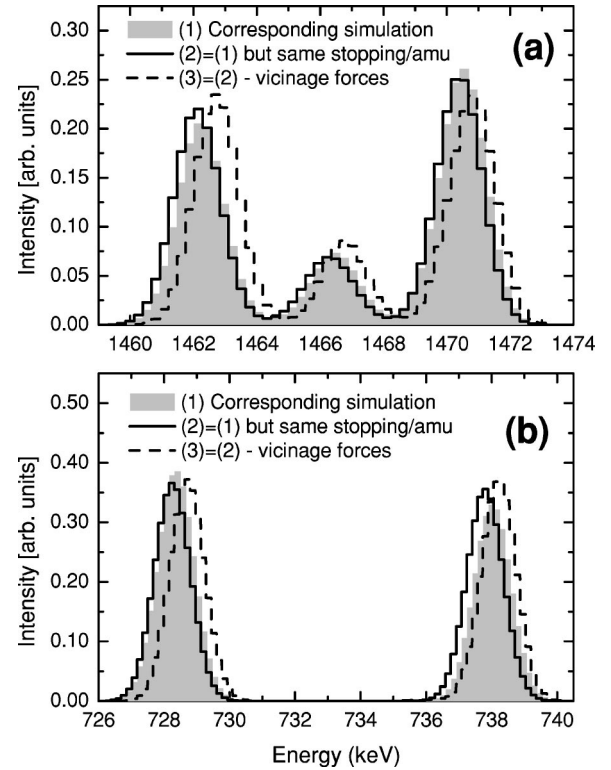

FIG. 6. Simulations of the dissociated fragments energy spectra for the experiment of Ref. [48]. The shadow histograms correspond to the complete simulation (Fig. 5); full line histograms were obtained using the same stopping per amu for all fragments; dashed line histograms are the same as full line ones but without using vicinage forces. (a) H_2^+ energy spectrum and (b) H^+ energy spectrum.

tion of H_2^+, putting the stopping per amu of H^+ ions equal to the value for H_2^+ but without considering H_2^+-H^+ vicinage force. Now Fig. 6(a) (dashed line) shows that the height difference between Coulomb peaks totally disappears, so vicinage force makes an additional contribution to the asymmetry. The fact that the H_2^+-H^+ vicinage force effects are opposite to the H^+-H^+ vicinage force effects is due to the difference in mass of the two particles resulting in the H_2^+ $+H^+$ dissociation. The vicinage force tends to align more efficiently the lighter particle behind the heavier one. This feature can be seen in the energy spectrum of the dissociated protons, Fig. 6(b). When we calculate the H^+ energy distribution putting H^+ stopping per amu equal to the H_2^+ value (full line), we see that vicinage forces produce a height difference in Coulomb peaks opposed to the height difference seen in the H_2^+ energy spectrum.

To sum up, the height asymmetry in Coulomb peaks of the energy spectra of different fragments from dissociated molecular ions is due to different electronic stopping per amu of the fragments and also due to the vicinage forces between them, because they produce different alignment depending on the fragment relative masses.

V. CONCLUSIONS

Vicinage forces for the cases H^+-H^+, H^+-H^0, H^0-H^0, and H_2^+-H^+ have been calculated using the dielectric formalism

and an energy-loss function developed by our group that describes properly the electronic stopping of the target material.

Vicinage forces tend to align the dissociated fragments from the molecular ions in the beam direction. This effect is shown clearly in the asymmetric heights of the Coulomb peaks that appear in the energy spectra of the dissociated fragments from the H_2^+ or H_3^+ molecules. This has been seen in H^+ energy distributions exiting at zero angle from the dissociation of H_2^+ ions, this asymmetry decreases when the fraction of H^0 is included in the simulation code calculation confirming that H^+-H^0 and H^0-H^0 vicinage forces are smaller than H^+-H^+ ones, and also confirming that these vicinage forces have to be taken into account to obtain the same results as the experimental ones.

Also the H_2^+ energy spectrum resulting from H_3^+ ions presents an asymmetry in the height of the Coulomb peaks but opposite to the one found in the later case. It has been demonstrated that the opposed asymmetry is due to two effects; the first one is that H_2^+ ions have smaller electronic stopping per amu than their proton dissociated partners, and the second one is that vicinage forces align more efficiently lighter particles behind heavier ones.

[1] J. Remillieux, Nucl. Instrum. Methods **170**, 31 (1980).

[2] E. Fermi, Phys. Rev. **57**, 485 (1940).

[3] J. Lindhard, K. Dan. Vidensk. Selsk. Mat. Fys. Medd. **28**, 8 (1954).

[4] J. Lindhard and A. Winther, K. Dan. Vidensk. Selsk. Mat. Fys. Medd. **34**, 8 (1963).

[5] D. Penn, Phys. Rev. **128**, 2093 (1962).

[6] W. Brandt and J. Reinheimer, Phys. Rev. B **2**, 3104 (1970).

[7] J.P. Walter and M.L. Cohen, Phys. Rev. B **5**, 3101 (1972).

[8] R.H. Ritchie and A. Howie, Philos. Mag. **36**, 463 (1977).

[9] I. Abril, R. Garcia-Molina, and N.R. Arista, Nucl. Instrum. Methods Phys. Res. B **90**, 72 (1994).

[10] D.J. Planes, R. Garcia-Molina, I. Abril, and N.R. Arista, J. Electron Spectrosc. Relat. Phenom. **82**, 23 (1996).

[11] I. Abril, R. Garcia-Molina, C.D. Denton, F.J. Pérez-Pérez, and N.R. Arista, Phys. Rev. A **58**, 357 (1998).

[12] J.C. Moreno-Marín, I. Abril, and R. Garcia-Molina, Nucl. Instrum. Methods Phys. Res. B **193**, 30 (2002).

[13] N.D. Mermin, Phys. Rev. B **1**, 2362 (1970).

[14] N.R. Arista, Nucl. Instrum. Methods Phys. Res. B **164**, 108 (2000).

[15] S. Heredia-Avalos, R. Garcia-Molina, and N.R. Arista, Europhys. Lett. **54**, 729 (2001).

[16] Z.L. Miskovic, S.G. Davison, F.O. Goodman, W.K. Liu, and Y.N. Wang, Phys. Rev. A **63**, 022901 (2001).

[17] C.D. Denton, M.D. Barriga-Carrasco, R. Garcia-Molina, K. Kimura, I. Abril, and N. R. Arista (unpublished).

[18] R. Garcia-Molina, S. Heredia-Avalos, and I. Abril, J. Phys.: Condens. Matter **12**, 5519 (2000).

[19] R. Laubert and F.K. Chen, Phys. Rev. Lett. **40**, 174 (1978).

[20] M.J. Gaillard, D.S. Gemmell, G. Goldring, I. Levine, W.J. Pietsch, J.C. Poizat, A.J. Ratkowski, J. Remillieux, Z. Vager, and B.J. Zabransky, Phys. Rev. A **17**, 1797 (1978).

[21] D.S. Gemmell, Chem. Rev. (Washington, D.C.) **80**, 301 (1980).

[22] W.P. Pietsch, D.S. Gemmell, P.J. Cooney, E.P. Kanter, D. Kurath, A.J. Ratkowski, Z. Vager, and B.J. Zabransky, Nucl. Instrum. Methods **170**, 61 (1980).

[23] J. Cooney, D.S. Gemmell, E.P. Kanter, W.J. Pietsch, and B.J. Zabransky, Nucl. Instrum. Methods **170**, 73 (1980).

[24] G.J. Kumbartzki, H. Neuburger, H.-P. Kohl, and W. Polster, Nucl. Instrum. Methods Phys. Res. **194**, 291 (1982).

[25] R. Garcia-Molina, C.D. Denton, I. Abril, and N.R. Arista, Phys. Rev. A **62**, 012901 (2000).

[26] C.D. Denton, R. Garcia-Molina, I. Abril, and N.R. Arista, Nucl. Instrum. Methods Phys. Res. B **135**, 45 (1998).

[27] C.D. Denton, R. Garcia-Molina, I. Abril, and N.R. Arista, Nucl. Instrum. Methods Phys. Res. B **135**, 50 (1998).

[28] R. Garcia-Molina, I. Abril, C.D. Denton, and N.R. Arista, Nucl. Instrum. Methods Phys. Res. B **164−165**, 310 (2000).

[29] R. Garcia-Molina, C.D. Denton, F.J. Pérez-Pérez, I. Abril, and N.R. Arista, Phys. Status Solidi B **219**, 23 (2000).

[30] L.D. Landau and E.M. Lifshitz, *Electrodynamics of Continuous Media* (Pergamon, Oxford, 1960).

[31] J.A. Phillips, Phys. Rev. **97**, 404 (1955).

[32] S.K. Allison, Rev. Mod. Phys. **30**, 1137 (1958).

[33] S. Kreussler and R. Sizmann, Phys. Rev. B **26**, 520 (1982).

[34] N.V. de Castro Faria, F.L. Freire, Jr., E.C. Montenegro, and A.G. De Pinho, J. Phys. B **19**, 1781 (1986).

[35] M. Farizon, N.V. de Castro Faria, B. Farizon Mazuy, and M.J. Gaillard, Phys. Rev. A **55**, 335 (1997).

[36] T. Kaneko, Phys. Rev. A **51**, 535 (1995).

[37] M.D. Barriga-Carrasco, Ph.D. thesis, Universidad de Murcia, 2002 (unpublished).

[38] N. Cue, N.V. de Castro Faria, M.J. Gaillard, J.C. Poizat, and J. Remillieux, Nucl. Instrum. Methods **170**, 67 (1980).

[39] Y. Susuki, M. Fritz, K. Kimura, M. Mannami, N. Sakamoto, H. Ogawa, I. Katayama, T. Noro, and H. Ikegami, Phys. Rev. A **50**, 3533 (1994).

[40] N. Cue, N.V. de Castro Faria, M.J. Gaillard, J.C. Poizat, and J. Remillieux, Phys. Lett. **72A**, 104 (1979).

[41] Y. Susuki, M. Fritz, K. Kimura, M. Mannami, N. Sakamoto, H. Ogawa, I. Katayama, T. Noro, and H. Ikegami, Phys. Rev. A **51**, 3868 (1995).

[42] W. Möller, G. Pospiech, and G. Schrieder, Nucl. Instrum. Methods **130**, 265 (1975).

[43] M. Nastasi, J.W. Mayer, and J.K. Hirvonen, *Ion-Solid Interac-*

tions (Cambridge University Press, Cambridge, 1996).

[44] W.L. Walters, D.G. Costello, J.G. Skofronick, D.W. Palmer, W.E. Kane, and R.G. Herb, Phys. Rev. **125**, 2012 (1962).

[45] C.D. Denton, I. Abril, M.D. Barriga-Carrasco, R. Garcia-Molina, G.H. Lantschner, J.C. Eckardt, and N.R. Arista, Nucl. Instrum. Methods Phys. Res. B **193**, 198 (2002).

[46] E.P. Kanter, P.J. Cooney, D.S. Gemmell, K.-O. Groeneveld, W.J. Pietsch, A.J. Ratkowski, Z. Vager, and B.J. Zabransky, Phys. Rev. A **20**, 834 (1979).

[47] T.R. Fox, K. Lam, and R. Levi-Setti, Nucl. Instrum. Methods Phys. Res. **194**, 285 (1982).

[48] N. Cue, M.J. Gaillard, J.C. Poizat, J. Remillieux, and J.L. Subtil, Phys. Rev. Lett. **42**, 959 (1979).